The Journal of Experimental Biology 207, 3265-3279
Published by The Company of Biologists 2004
doi:10.1242/jeb.01139

The hydrodynamics of eel swimming

II. Effect of swimming speed

Eric D. Tytell

Department of Organismic and Evolutionary Biology, Harvard University, Cambridge, MA 02138, USA

e-mail: tytell@oeb.harvard.edu

Accepted 10 June 2004

Summary

Simultaneous swimming kinematics and hydrodynamics are presented for American eels, *Anguilla rostrata*, swimming at speeds from 0.5 to 2 L s^{-1}. Body outlines and particle image velocimetry (PIV) data were collected using two synchronized high-speed cameras, and an empirical relationship between swimming motions and fluid flow is described. Lateral impulse in the wake is estimated assuming that the flow field represents a slice through small core vortex rings and is shown to be significantly larger than forces estimated from the kinematics *via* elongated body theory (EBT) and *via* quasi-steady resistive drag forces. These simple kinematic models predict only 50% of the measured wake impulse, indicating that unsteady effects are important in undulatory force production. EBT does, however, correctly predict both the magnitude and time course of the power shed into the wake. Other wake flow structures are also examined relative to the swimming motions. At all speeds, the wake contains almost entirely lateral jets of fluid, separated by an unstable shear layer that rapidly breaks down into two vortices. The jet's mean velocity grows with swimming speed, but jet diameter varies only weakly with swimming speed. Instead, it follows the body wavelength, which changes more among individuals than at different speeds. Circulation of the stop–start vortex, shed each time the tail changes direction, can also be predicted at low speeds by the integral of squared tail velocity over half of a tail beat. At high speeds, these kinematics predict more circulation than is actually present in the stop–start vortex. Finally, the cost of producing the wake, one component of the total cost of transport, increases with swimming speed to the 1.48 power, lower than would be expected if the power coefficient remained constant over the speed range examined.

Key words: eel, *Anguilla rostrata*, wake structure, particle image velocimetry, fish, fluid dynamics, efficiency, swimming speed, kinematics.

Introduction

For most of the past century, fish swimming studies have focused on how fish move when they swim. Early studies classified different modes of swimming (Marey, 1895; Breder, 1926) and developed physical theories on how swimming motions could produce thrust (Gray, 1933; Taylor, 1952; Lighthill, 1960; Wu, 1971). More recent work has examined swimming kinematics quantitatively, describing how the kinematics change at different speeds (Webb, 1975, 1991; Jayne and Lauder, 1995; Donley and Dickson, 2000) and between different fish species (Videler and Hess, 1984; Webb, 1988; Webb and Fairchild, 2001). Many kinematic studies have applied Lighthill's elongated body theory (EBT; Lighthill, 1960, 1971) to the measured swimming kinematics in order to predict thrust and drag forces, power and efficiency (e.g. Weihs, 1972; Webb, 1975, 1988, 1992; Videler and Hess, 1984; Pedley and Hill, 1999). Recently, it has become possible to quantitatively measure the fluid flow around a fish as it swims, which allows a more straightforward estimation of forces and powers and provides a check for theoretical models. While the flow around swimming fishes has also been studied for many years (e.g. Rosen, 1959; Aleyev, 1977; McCutchen, 1977), it is only recently that the flow around swimming fishes has been examined quantitatively (Anderson, 1996; Müller et al., 1997, 2001; Drucker and Lauder, 2001; Nauen and Lauder, 2002a,b). Despite the long history of swimming kinematics research, these hydrodynamic studies have generally included little kinematic data from the fishes they studied.

Nonetheless, the diversity of wakes observed from swimming fishes to some extent reflects the standard classification of swimming modes (Breder, 1926). Carangiform and subcarangiform swimmers produce a single vortex each time the tail changes direction, resulting in a wavy jet, pointing downstream, between the vortices. Anguilliform swimmers produce a rather different wake. As originally observed by Müller et al. (2001) and described in detail in Part

I of this study (Tytell and Lauder, 2004), eels produce two same-sense vortices each time the tail moves from one side to the other and do not produce any substantial downstream flow. Connecting these hydrodynamic differences to kinematic differences remains difficult, in part because of the diverse morphologies and evolutionary histories of fish with different swimming modes.

A better way to examine how different body movements affect hydrodynamics is to examine changes in kinematics and hydrodynamics over a range of speeds in the same species. Several hydrodynamic studies identify interesting changes in the wake at different speeds. In particular, Nauen and Lauder (2002a) described a substantial reorientation of vortex rings in mackerel wakes as they increased speed. Clearly, the mackerel must be changing their swimming motions to produce these hydrodynamic changes. While mackerel swimming kinematics have been studied at a range of speeds (Videler and Hess, 1984; Donley and Dickson, 2000), how the kinematics cause this reorientation is not clear. Also, Drucker and Lauder (2000) documented substantial changes in the wakes of two pectoral fin swimmers – bluegill sunfish and black surf perch – as they increased swimming speed. Surf perch showed a reorientation of vortex rings at higher speeds, and bluegill began to generate an entirely new ring above a certain speed. Pectoral fin kinematics have also been examined (Webb, 1973) separately from the hydrodynamics but, without simultaneous measurements of fin motions and flow fields, explaining how different kinematics cause the hydrodynamic changes is difficult.

These previous studies have described how the flow behind various swimming fishes looks and how it changes with swimming speed, but simultaneous observation of kinematics and hydrodynamics can begin to explain why the flow changes the way it does. In the present study, therefore, I examine the empirical relationship between swimming kinematics and hydrodynamics in steadily swimming eels, *Anguilla rostrata*, at a range of speeds from ~0.5 to 2 body lengths per second (L s^{-1}).

Materials and methods

The experimental method used for this paper is the same as described in Part I of this study (Tytell and Lauder, 2004). It is summarized briefly below, with differences from Part I noted. American eels (*Anguilla rostrata* LeSueur) from the Charles river (Cambridge, MA) were allowed to swim on the bottom of a recirculating flow tank at a range of speeds from ~0.5 to 2.0 L s^{-1}. In Part I, only one speed was studied. Not all individuals would swim consistently at the lowest or highest speed; speed was increased or decreased, respectively, until consistent steady swimming was achieved. Considerable effort was taken to ensure that all individuals were swimming steadily at all speeds. At most, swimming speed varied from the oncoming flow speed by less than 7% and usually varied by less than 2%. The swimming speed was therefore assumed to be equal to the flow speed, on average. Each swimming sequence included at least five sequential, steady tail beats and most had $\geqslant$10.

A single laser light sheet, produced using two argon-ion lasers at 4 and 8 W, respectively, was focused 7 mm above the tank bottom. Eels only swam steadily on the bottom of the flow tank, which required the laser to be this close to the bottom. A detailed analysis of the flow tank boundary layer was performed and is reported in Tytell and Lauder (2004). At this height, the light sheet illuminated the plane along the dorso-ventral midline of the eel but was above the turbulent boundary layer of the flow tank.

The light sheet and the swimming kinematics were filmed from below using two high-speed digital cameras, one focused on the eel (RedLake; 250 or 125 Hz, 480×420 pixels) and the other focused on the light sheet behind the eel (either RedLake or NAC Hi-DCam at 250 Hz, 480×420 pixels or 500 Hz, 1280×1024 pixels, respectively). Additionally, the snout and tail tip were digitized manually, which allowed a custom Matlab 6.5 (MathWorks, Inc., Natick, MA, USA) program to digitize 20 points along the eel midline automatically. Kinematic parameters, such as tail beat amplitude and frequency, were calculated from the timing and amplitude of each peak in lateral excursion along the midline. Following Gillis (1997), three angles were calculated for the posterior 5% of the body: its angle relative to the swimming direction (the tail angle); the angle of its path of motion relative to the swimming direction (the path angle); and its instantaneous angle of attack. Strouhal number was also estimated as $2fA/U$ (Triantafyllou et al., 1993), where f and A are the tail beat frequency and amplitude, respectively, and U is the swimming speed. Strouhal number has been shown to be strongly indicative of the force production and efficiency of flapping foils (Read et al., 2003) and may have a similar importance for undulatory locomotion.

Another Matlab program performed two-pass digital particle image velocimetry (PIV) as in Hart (2000) but using a statistical correlation function (Fincham and Spedding, 1997). Vortex centers were digitized manually, and vortex circulation was calculated by integrating along a contour 8 mm from the center. Finally, the mean flow was calculated in a 8×8 mm region, centered 12 mm behind the tail tip.

Force, power and impulse were estimated from both the kinematics and the flow field. Large-amplitude EBT (Lighthill, 1971), a reactive model, was used to estimate thrust and lateral forces and power required to produce the wake from the kinematic, as follows:

$$F_{\mathrm{L,react}} = \left[-mv_{\perp}\left(\frac{\partial x_{\mathrm{b}}}{\partial t} + U\right) + \tfrac{1}{2}mv_{\perp}^{2}\frac{\partial y_{\mathrm{b}}}{\partial s}\right]_{s=L} - \frac{\partial}{\partial t}\int_{0}^{L} mv_{\perp}\frac{\partial y_{\mathrm{b}}}{\partial s}\,\mathrm{d}s\,, \tag{1}$$

$$P_{\mathrm{react}} = [\tfrac{1}{2}mv_{\perp}^{2}v_{\parallel}]_{s=L}\,, \tag{2}$$

where $x_{\mathrm{b}}(s,t)$ and $y_{\mathrm{b}}(s,t)$ are the positions of points along the

midline of an eel facing in the positive x direction in flow with speed U towards the eel, m is the virtual mass per unit length, L is the eel's length, t is time and s is the distance along the midline from head to tail. The body velocities $v_\perp$ and $v_\parallel$ are perpendicular and parallel to the midline, respectively. In addition, resistive forces were calculated by summing the quasi-steady drag forces normal and tangential to the body midline using the true kinematics, in a similar way to Jordan (1992). This force is:

$$F_{\mathrm{L,resist}} = \tfrac{1}{2}\rho \int_0^L [(C_{\mathrm{D},\perp} h v_\perp^2)\cos\theta + (C_{\mathrm{D},\parallel} h v_\parallel^2)\sin\theta]\, \mathrm{d}s\,, \quad (3)$$

where h is the eel's height, ρ is fluid density, $v_\perp$ and $v_\parallel$ are the fluid velocities normal and tangential to a segment, taking into account the segment's own motion, and θ is the angle of the segment relative to the path of motion. The normal and tangential drag coefficients $C_{\mathrm{D},\perp}$ and $C_{\mathrm{D},\parallel}$ were estimated according to empirical descriptions of turbulent flow normal to a cylinder (Taylor, 1952; Hoerner, 1965) and parallel to a flat plate (Hoerner, 1965), respectively, under steady conditions:

$$C_{\mathrm{D},\perp} = 1.2 + 4Re_{\mathrm{n}}^{-0.5},\ Re_{\mathrm{n}} = hv_\perp/\nu\,, \quad (4)$$

$$C_{\mathrm{D},\parallel} = 0.37(\log Re_{\mathrm{x}})^{-2.6},\ Re_{\mathrm{x}} = xv_\parallel/\nu\,, \quad (5)$$

where Re is Reynolds number. Wake power was not calculated from the resistive model because it does not explicitly account for how power is shed into the wake. Simply integrating power, like force, neglects the fact that fluid must flow over different periods of time into the wake. Without substantially complicating the model, there is no way to calculate wake power.

Lateral impulse from reactive (EBT) and resistive force estimates was calculated by integrating forces over half a tail beat. These estimates were compared with the same values measured using PIV. Assuming that vortex pairs in the wake were separate vortex rings, the ring circulation was also calculated by integrating along a line equidistant from the vortex pairs. Ring impulse (I_{ring}) and force (F_{ring}) were estimated as:

$$I_{\mathrm{ring}} = (\pi/4)\rho\Gamma h d\,, \quad (6)$$

$$F_{\mathrm{ring}} = 2I_{\mathrm{ring}} f\,, \quad (7)$$

where ρ is the water density, Γ is the circulation, d is the distance between the vortex pairs, h is the dorsoventral height of the eel, and f is the tail beat frequency. Impulse generated at the tail tip was also estimated from the first moment of vorticity (Birch and Dickinson, 2003), averaged over half a tail beat:

$$I_{\mathrm{vort}} = \rho h \int_A \mathbf{r} \times \boldsymbol{\omega}\, dA\,, \quad (8)$$

where ρ is the fluid density, $\mathbf{r}$ is the position vector from the tail tip, ω is the vorticity vector, and A is the area of the light sheet. Because only a single horizontal plane was examined, this expression assumes that vorticity is the same in all horizontal planes over the height of the eel. Force was estimated by taking the time derivative of I_{vort} (Birch and Dickinson, 2003). The power required to produce the wake was determined by integrating the kinetic energy flux through a 80×10 mm plane, 8 mm behind the eel, and subtracting the kinetic energy flux upstream of the eel, based on the mean flow velocity. Additionally, a 'lateral' power was estimated by assuming the small and relatively noisy axial component of velocity was zero and integrating only the lateral velocity contribution to the kinetic energy flux. Phasing of the wake power was adjusted by $2\pi x_{\mathrm{plane}}/Uf$, where x_{plane} (=8 mm) is the distance between the tail tip and the plane where power was estimated, to account for the phase lag between when the kinetic energy was shed at the tail and when it reached x_{plane}.

The cost of producing the wake was estimated by dividing the wake power by the swimming speed. This cost is one component of the total mechanical cost of transport, which also includes the thrust power and the inertial power required to undulate the body.

Forces, powers and impulses were normalized to produce non-dimensional coefficients by dividing by $\frac{1}{2}\rho SU^2$, $\frac{1}{2}\rho SU^3$ and $\frac{1}{2}\rho SLU$, respectively (Schultz and Webb, 2002; Tytell and Lauder, 2004), where S is the wetted surface area of the eel, L is the eel's length and U is the swimming speed.

All statistics were performed in Systat 10.1 (Systat Software, Point Richmond, CA, USA). All errors listed are standard error. A three-way, mixed-model analysis of variance (ANOVA; Milliken and Johnson, 1992) was performed to compare impulse estimates from PIV and theoretical models. Forces were not compared directly because of the uncertainty in estimating the generation time in equations 6, 7. Instead, by comparing impulse, the mean force output over a tail beat was compared without the problem of when that force was generated. In the ANOVA, the fixed factors were type of measurement and swimming speed (slow, moderate and fast), and the random factor was individual. Measurement type had five values: vortex ring impulse from PIV (abbreviated as PVR); direct integration of vorticity (PDIV); impulse from the reactive model (KEBT); impulse from the resistive model (KRES) and the sum of the reactive and resistive impulses (KBOTH). Four comparisons were planned in advance: PVR with PDIV, PVR with KEBT, PVR with KRES and PVR with KBOTH. Because these differences were expected *a priori*, the same type of F test used to test for differences among all group members was used to compare them individually (Milliken and Johnson, 1992).

A similar ANOVA was performed to compare mean power estimates but with only three types of measurement: total power from PIV (PTOT); lateral power from PIV (PLAT) and wake power from the reactive (EBT) model (KEBT). Planned comparisons were PTOT with KEBT and PLAT with KEBT.

Other regressions were performed with 'individual' as a dummy variable, and significance tested including it as a random effect (Milliken and Johnson, 2001).

Results

In total, the kinematics and hydrodynamics of 11 individuals with total lengths from 12 to 24 cm were examined qualitatively at speeds from ~0.5 to 2 L s^{-1}. From these, three individuals (lengths of 20 cm, 20 cm and 23 cm, corresponding to masses of 14 g, 16 g and 14 g) that swam particularly steadily were selected for detailed analysis. The kinematics and hydrodynamics of 274 tail beats were analyzed. The swimming sequences were divided into four speed categories: very slow (0.549±0.007 L s^{-1}; N=17); slow (0.906±0.005 L s^{-1}; N=56); moderate (1.374±0.003 L s^{-1}; N=118) and fast (1.88±0.01 L s^{-1}; N=83). Only one individual swam steadily at the slowest speed. Because this resulted in an extremely unbalanced statistical layout, all data at this speed were excluded from statistical analyses in which both individual and speed were treated categorically (Milliken and Johnson, 1992).

Kinematics

Because the wake was quite sensitive to changes in swimming movements, the kinematics were quantified in detail (Fig. 1; Table 1). Tail beat amplitude and frequency were poorly correlated with swimming speed (r^2=0.372 and

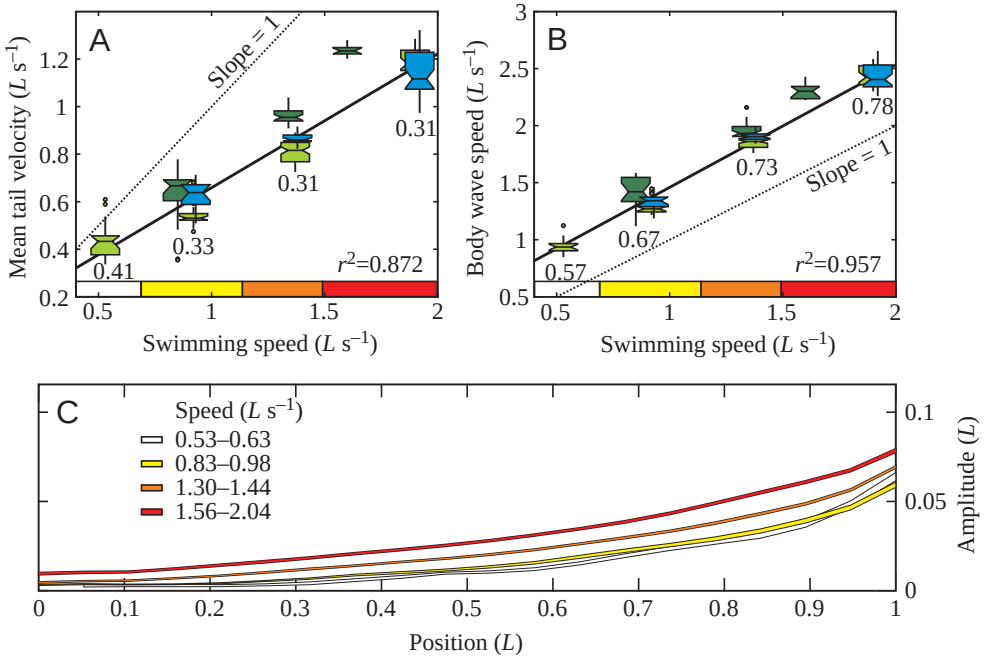

Fig. 1. Swimming kinematics. Shades from white to red represent different swimming speeds, and shades of blue and green represent different individuals. In A and B, the boxes are standard statistical box plots, with the box stretching from the 25th to 75th quartile, which identifies where 50% of the data lie, and a line at the median. The error bars above and below each box reach to the maximum or minimum values or 1.5 times the size of the box, whichever is smaller. Any points that are beyond the length of the error bars are identified as outliers and shown as separate points. The narrow areas along the boxes represent approximate 95% confidence intervals. (A) Mean tail velocity, U_{tail}, equal to 4Af, where A and f are the tail beat amplitude and frequency, respectively, against swimming speed (U). Solid line, linear regression; dotted line, slope of one. Mean Strouhal number (2Af/U) is shown for each speed. (B) Body wave speed, V, against swimming speed. Solid line, linear regression; dotted line, slope of one. Slip (U/V) is shown below each speed. (C) Undulation amplitude, defined as half the total body excursion at each point along the body at the four swimming speeds. Thickness of the line represents standard error.

Table 1. *Regressions against swimming speed*

Variable	Constant	Slope	R^2	$F_{1,2}$	P
Kinematics					
Amplitude (L)	0.0699±0.0006		0.372	8.93	0.096[a]
Frequency (Hz)	1.3±0.10	+1.30±0.07	0.572	26.35	0.036[a]
Wavelength (L)	0.597±0.005		0.215	13.48	0.067
Tail velocity (L s^{-1})	0.09±0.02	+0.56±0.01[b]	0.872	110.8	0.009[a]
Wave speed (L s^{-1})	0.39±0.02	+1.07±0.01[b]	0.957	2381.0	0.0004
Strouhal number	0.324±0.003		0.172	4.39	0.171
Hydrodynamics					
Jet magnitude (L s^{-1})	0.20±0.01	+0.122±0.008	0.461	21.29	0.044
Jet angle (deg.)	89.43±0.01[c]		0.355	0.83	0.458
Jet diameter (L)	0.205±0.001		0.136	4.98	0.155

Regression coefficients are for joint regression across all individuals. Only the overall mean value is listed for non-significant regressions. F and P values are for the effect of swimming speed, including individual as a random effect. Individual is significant (P<0.05) in all regressions.
[a]N=275; [b]significantly different from 1 (P<0.05); [c]not significantly different from 90 (P=0.407).

0.572, respectively), particularly at low speeds, and both varied by as much as 20% in most sets (S.D.=8%). In addition, amplitude was not significantly correlated with swimming speed when individual was included as a random effect (P=0.096; Table 1). However, at a given swimming speed, amplitude and frequency were approximately inversely proportional to each other (Fig. 2), so that the mean tail velocity was well correlated with swimming speed (r^2=0.872; Fig. 1A). This correlation means that Strouhal number, $2fA/U$ (Triantafyllou et al., 1993), stays approximately constant at 0.324±0.003. No significant change was observed in Strouhal number with swimming speed ($F_{1,2}$=4.39, P=0.171), and the eels seem to maintain Strouhal number within a swimming speed (Fig. 2). Individuals do not have significantly different Strouhal numbers ($F_{2,268}$=0.151, P=0.860). Even though amplitude was not significantly related to swimming speed ($F_{1,2}$=8.93, P=0.096), it tended to increase with swimming speed at all points on the body, increasing fastest at the head (Fig. 1C). Body wave speed was tightly correlated with swimming speed (r^2=0.957) and increased slightly faster than the swimming speed (Fig. 1B; $F_{1,2}$=26.12, P=0.036). The ratio of swimming speed to body wave speed, called slip, thus increased from 0.57±0.01 at the slowest speed to 0.784±0.002 at the highest. Body wave length was, on average, 0.597±0.005 and did not change significantly with swimming speed ($F_{1,2}$=13.48, P=0.067), although it did show a trend to increase at higher speeds. The largest variation in body wave length was due to individual variation, resulting in differences of as much as 30% between individuals.

At a given swimming speed, amplitude increased along the body exponentially. All logarithmic regressions had r^2 values higher than 0.970, while the linear regression r^2 values were always less than 0.2. The lateral (y) position of the midline could be accurately described as:

$$y(s) = Ae^{\alpha(s/L-1)} \sin\left[\frac{2\pi}{\lambda}(s - Vt)\right], \quad (9)$$

where s is the contour length along the midline starting at the head, A is the tail beat amplitude, α is the amplitude growth rate, L is the body length, λ is body wave length, t is time and V is body wave speed. By this definition, a large α implies that amplitude is low near the head and increases rapidly near the tail. A smaller α implies more undulation anteriorly. To determine the α parameter at a given swimming speed, $\ln[y_{max}(s)/A]$ and y_{max}/A were regressed on s/L–1 without a constant. Based on the logarithmic regressions, α was equal to 3.90±0.04 at the lowest speed and decreased to 2.25±0.01 at the highest speed, showing an increase in body amplitude of 420% at the head at the highest speeds.

The maximum angle of attack of the tail decreased with increasing swimming speed (Fig. 3A). Additionally, at higher swimming speeds, the tail spent a lower fraction of the tail beat with a positive angle of attack (Fig. 3B), decreasing from 0.866±0.003 at the lowest speed to 0.786±0.003 at the highest. The tail generally reached its maximum angle of attack when it had the highest velocity, approximately as it crossed the path of motion.

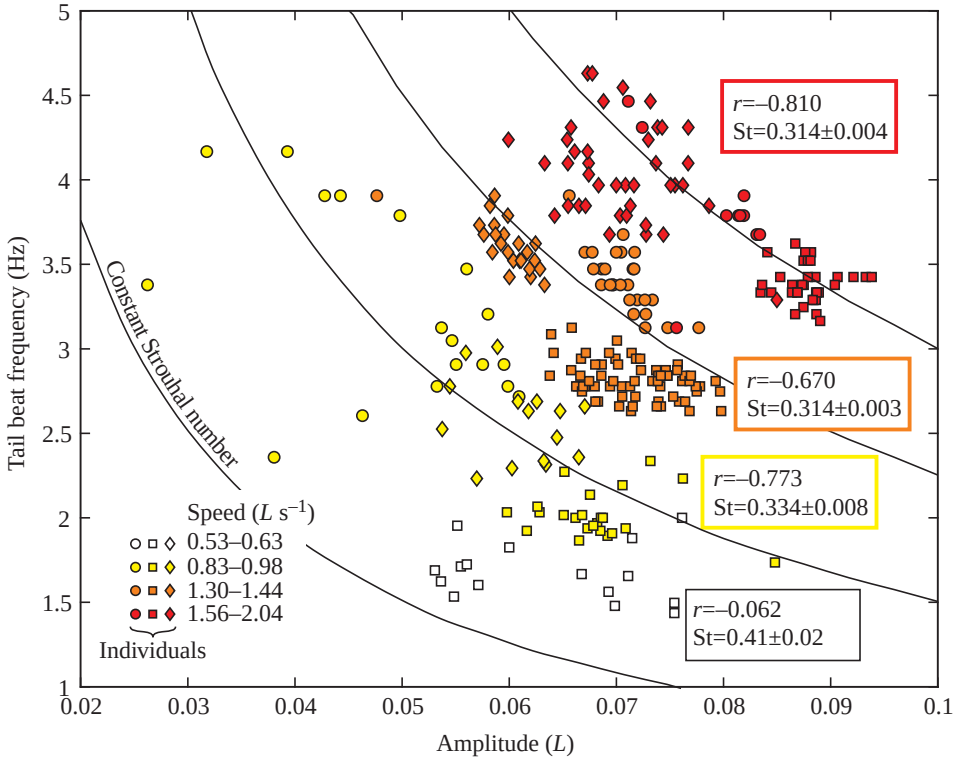

Fig. 2. Tail beat frequency against tail beat amplitude. Shades from white to red represent different swimming speeds, and marker shape indicates different individuals. Lines of constant 0.3 Strouhal number are shown in black. The correlation coefficient r and mean Strouhal number are shown for each swimming speed.

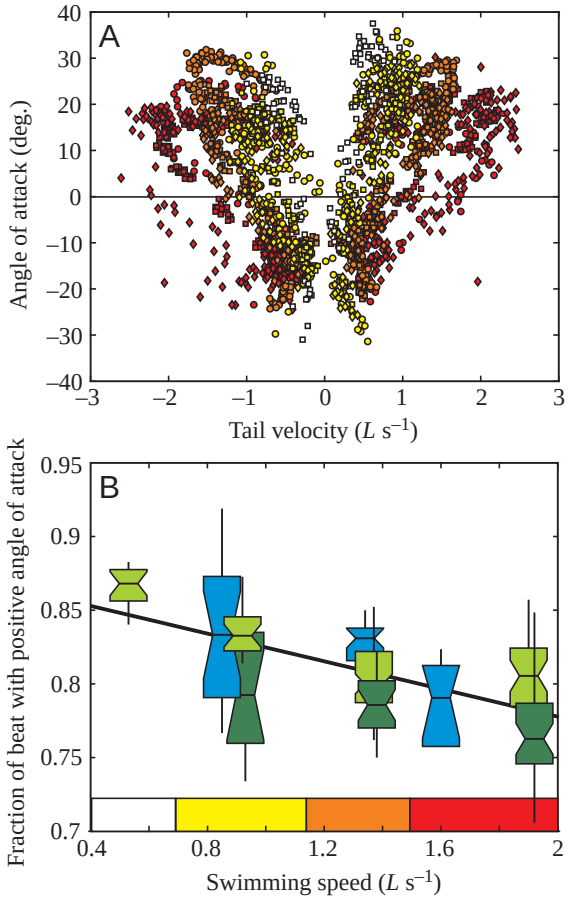

Fig. 3. Angle of attack of the tail. Shades from white to red represent increasing swimming speeds. (A) Angle of attack plotted against tail velocity over complete tail beats. Different shaped markers represent different individuals. (B) Fraction of the tail beat cycle in which the tail has a positive angle of attack plotted against swimming speed. Shades of blue and green represent different individuals. Boxes are standard statistical box plots, described in detail in Fig. 1.

Hydrodynamics

At all steady swimming speeds, the wake retained approximately the same form. The wake contains lateral jets of fluid, alternating in direction, separated by one or more vortices or a shear layer (Fig. 4). Each time the tail changes direction, it sheds a stop–start vortex. As the tail moves to the other side, a low pressure region develops in the posterior quarter of the body, sucking a bolus of fluid laterally. The bolus is shed off the tail, stretching the stop–start vortex into an unstable shear layer, which eventually rolls up into two or more separate, same-sign vortices. This pattern was consistent at all speeds, even though the strength of the lateral jet increased at higher speeds (Fig. 5).

The jet magnitude, direction and diameter were measured at the different swimming speeds (Fig. 5). Jet magnitude increased linearly (r^2=0.461) with swimming speed and had a significant slope (Table 1; $F_{1,2}$=21.29, P=0.044). Neither jet angle nor jet diameter had significant regressions against swimming speed when individual was treated as a random variable ($F_{1,2}$=0.83 and 4.98, respectively, corresponding to P=0.458 and 0.155). For each individual, jet diameter did tend to increase with swimming speed, which was shown by a significant interaction term between swimming speed and individual ($F_{2,268}$=24.17, P<0.001). Jet angle, on the other hand, was not significantly different from 90 at any speed (P=0.407), although the jet did have a tendency to point slightly upstream.

Although the jet diameter did not change significantly with swimming speed, it did have a significant relationship to the body wavelength (Fig. 6). One might expect that the jet diameter should be about half of a full wave on the body, because the bolus of fluid that becomes the jet forms in a half wave (Tytell and Lauder, 2004). However, Fig. 6 shows that the jet diameter is about a quarter wavelength (not significantly different from 0.25; $F_{1,268}$=1.044, P=0.308) and is significantly less than half a wavelength ($F_{1,268}$=133.4, P<0.001). Individual variation in body wavelength was as much as 30% at a specific swimming speed but, despite this variation, wake jet diameter remains correlated with body wavelength. For example, the individual represented by squares and solid lines in Fig. 6 consistently chose a longer body wavelength and, as a result, had wider jets than the others, even at lower swimming speeds.

The mean flow from an 8×8 mm region behind the tail tip was regressed on the tail tip velocity (Fig. 7). Tail tip velocity was used as the dependent variable, rather than swimming speed, because it allows variation within a swimming speed to be analyzed but is still highly correlated with swimming speed. Mean axial flow always pointed downstream, away from the eel, and increased linearly with increasing tail velocity (P<0.001, r^2=0.299). The mean lateral flow magnitude increased with swimming speed but had a significant nonlinear component. In a quadratic polynomial regression, both the linear and quadratic terms were significant (P<0.001 and P=0.002, respectively), and the constant was not significantly different from zero (P=0.807).

The vortices on either side of the lateral jet appear to be part of a small core vortex ring (Müller et al., 2001). Thus, by analogy with vortex ring generators (review in Shariff and Leonard, 1992), the total circulation added to the fluid by the tail should be:

$$\Gamma_{\mathrm{tail}} = \tfrac{1}{2}\int_{T_{\frac{1}{2}}} U_{\mathrm{t}}^2 \, \mathrm{d}t \,, \qquad (10)$$

where $T_{\frac{1}{2}}$ is a half tail beat, specifically from maximum lateral excursion on one side to the other side, and U_{t} is the tail tip velocity. Fig. 8 shows the maximum circulation of the primary vortex plotted against Γ_{tail}. At values of less than ~40 cm^2 s^{-1}, the two match well but, at higher values, Γ_{tail} tends to overestimate the measured circulation. A quadratic polynomial regression between the two had significant linear and quadratic terms (P<0.001 in both cases). The coefficient of the linear term was not significantly different from one (P=0.644).

The cost of producing the wake increases exponentially with

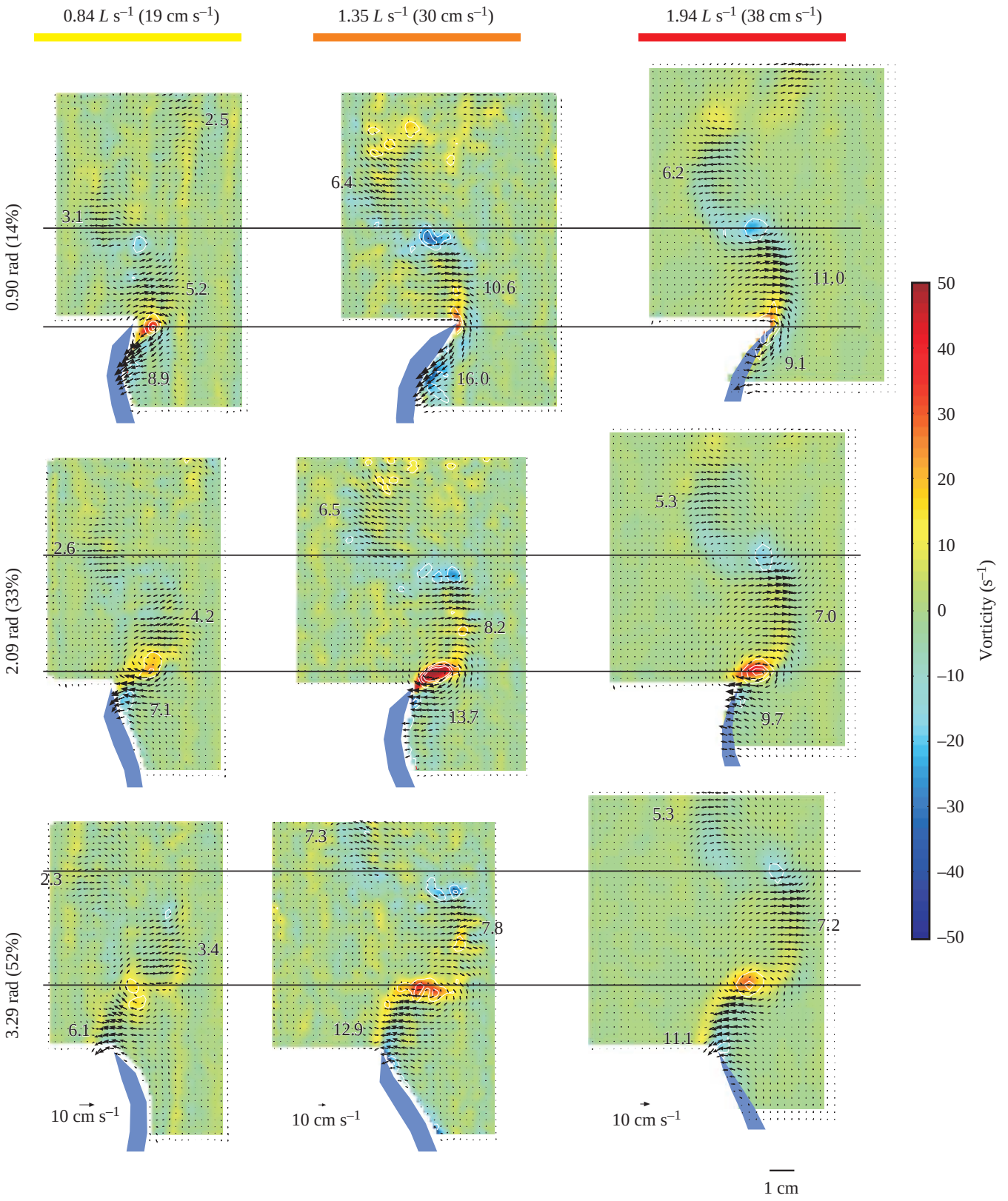

Fig. 4. Wake flow at three different swimming speeds and three different phases during the tail beat cycle. Black arrows represent flow velocity magnitude and direction. Vorticity is shown in color in the background, and contours of the discriminant for complex eigenvalues at –200, –500 and –1000 are shown in white. The eel's tail is in blue at the bottom. Note that the vector scale is different for each swimming speed but the length and vorticity scales are the same in all plots. Mean jet magnitude in $L\ s^{-1}$ is written beside each jet. Horizontal lines are provided to facilitate comparisons of jet diameter.

mean tail tip speed (Fig. 9). Again, mean tail speed was used as a proxy for swimming speed to highlight variation within a single swimming speed. Wake energy cost increased as the tail speed increased with an exponent of 1.48±0.03 (r^2=0.755, P=0.011). Individuals had significantly different exponents (P<0.001), especially the individual represented by circles, which had an exponent of 2.05±0.08. Because tail velocity is directly proportional to swimming speed, this regression means that wake energy cost also increases with swimming speed to the 1.48 power.

Finally, the predictions of Lighthill's reactive EBT (Lighthill, 1971) and a resistive model (Taylor, 1952; Jordan, 1992) were compared with the PIV measurements (Fig. 10; Table 2). All values were normalized to produce non-dimensional coefficients before comparison. A three-way mixed-model ANOVA was performed on impulse coefficient with fixed factors of swimming speed (~0.9, 1.4 and 1.9 L s^{-1}) and type of measurement (KEBT, KRES and KBOTH *vs* PVR and PDIV), and 'individual' as a random factor (Fig. 10A; Table 2). Because only one individual swam steadily at the slowest speed (0.55 L s^{-1}), the above test was required mathematically to exclude this speed, although it is shown in the figures for visual comparison. Swimming speed had no significant effect on the measurements (P=0.469) nor did the differences between types change at different speeds (P=0.189). Individuals were significantly different (P<0.001). The measurement types were also significantly different (P<0.001). *A priori* planned comparisons were conducted to compare certain measurement types using F tests (Quinn and Keough, 2002). In particular, vortex ring impulse (PVR) was significantly larger than all other methods of estimating impulse (P<0.001 in all cases).

Additionally, the axial force component of F_{vort} is not significantly different from zero. Based on an ANOVA with speed as the only factor, the axial component does not differ from zero at any speed ($F_{4,270}$=0.079, P=0.989).

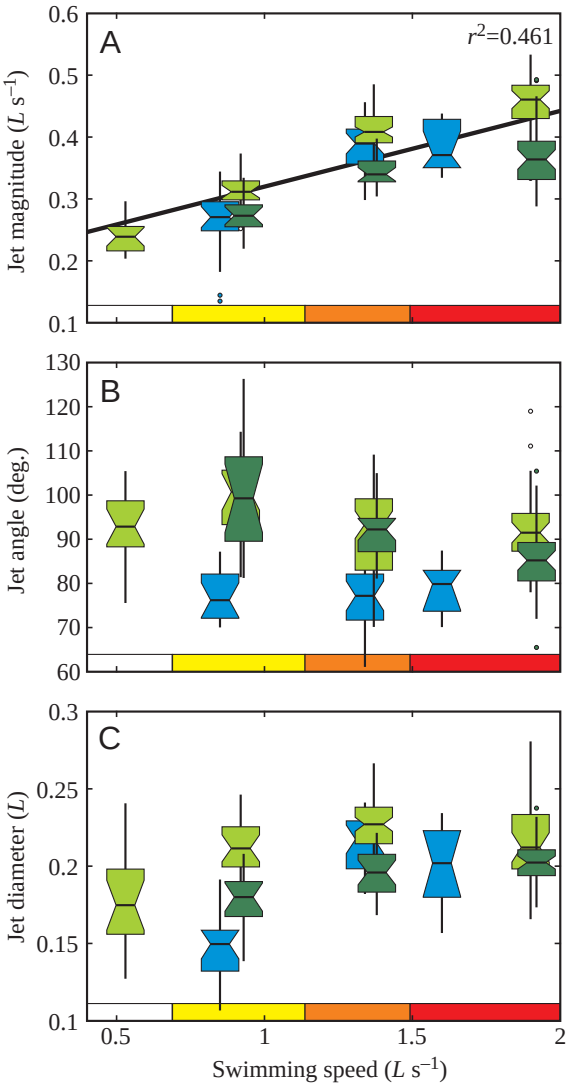

Fig. 5. Size, strength and angle of the lateral jets in the wake at different swimming speeds. Boxes are standard statistical box plots, described in detail in Fig. 1. Shades from white to red represent different swimming speeds, and shades of blue and green represent different individuals. (A) Mean jet velocity magnitude against swimming speed. A linear regression line is shown in black and the r^2 value is indicated above. (B) Mean angle of the jet against swimming speed. (C) Jet diameter against swimming speed. No significant linear relationship exists in B and C and so a regression line is not shown.

Table 2. *Comparison of elongated body theory with particle image velocimetry*

Value	*F*	*d.f.*	*P*
Lateral impulse*			
Type	**26.17**	**4,8**	**<0.001**
PVR with PDIV	**50.37**	**1,8**	**<0.001**
PVR with KEBT	**58.47**	**1,8**	**<0.001**
PVR with KRES	**90.03**	**1,8**	**<0.001**
PVR with KBOTH	**31.92**	**1,8**	**<0.001**
Speed	0.919	2,4	0.469
Type × speed	1.644	8,16	0.189
Individual†	**92.12**	**2,1238**	**<0.001**
Power‡			
Type	5.97	2,4	0.063
PTOT with KEBT	**7.90**	**1,4**	**0.048**
PLAT with KEBT	**0.11**	**1,4**	0.753
Speed	0.50	2,4	0.640
Type × speed	1.03	4,8	0.446
Individual†	**4.91**	**2,744**	**0.008**

Bold indicates a significant effect. Planned comparisons are listed individually under the effect 'Type'. *N=1285; †random effect; ‡N=771; PVR, impulse estimated from particle image velocimetry (PIV) data assuming small core vortex rings; PDIV, impulse estimated from PIV data by direct integration of vorticity; KEBT, impulse estimated from kinematics by elongated body theory; KRES, impulse estimated from kinematics by a resistive model; KBOTH, sum of KEBT and KRES; PTOT, total power from PIV data; PLAT, power including only contributions from lateral flow from PIV data; KEBT, power estimated from elongated body theory.

Mean power coefficients were compared in a similar ANOVA as impulse, again with five types of measurement (KEBT *vs* PTOT and PLAT; Fig. 10B; Table 2). Again, estimates did not change with swimming speed (P=0.623) nor did the differences between methods change at different speeds (P=0.331). Individuals were significantly different (P<0.001). Differences between measurement types were marginally non-significant (P=0.063). At this level of significance, planned comparisons can still be conducted (Quinn and Keough, 2002), revealing that the mean total power coefficient from PIV

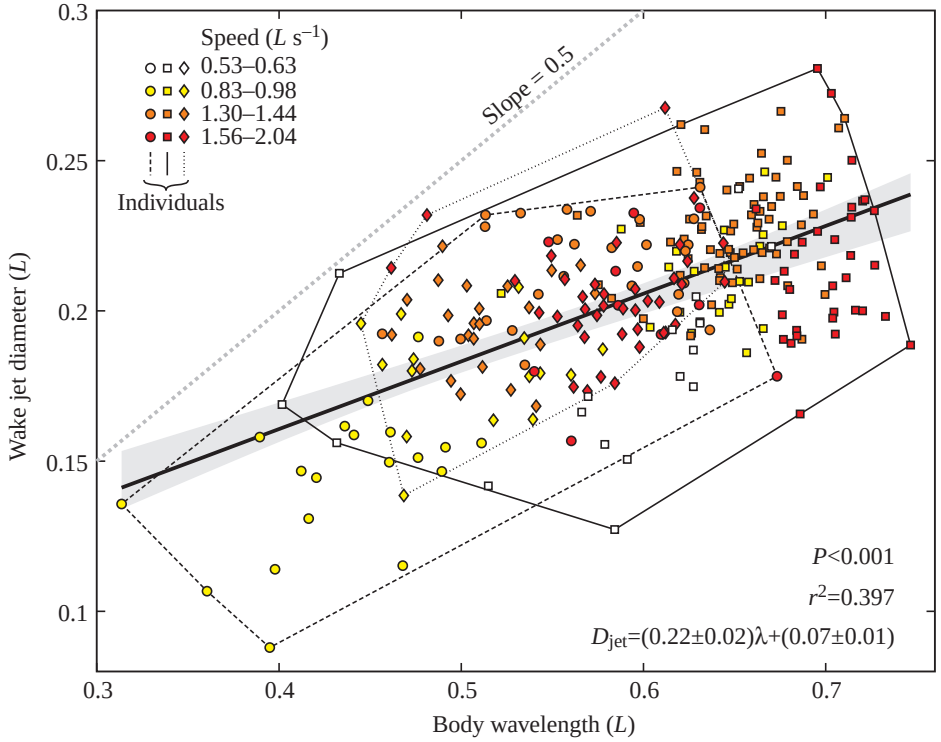

Fig. 6. Relationship of the wake jet diameter to body wavelength. Shades from white to red represent different swimming speeds, and marker shape indicates different individuals. The convex hull containing each individual's points is shown with thin black lines. A linear regression line is shown with a thick black line, and a gray dotted line indicates a slope of 0.5. The P and r^2 values, and the regression equation, are given in the corner.

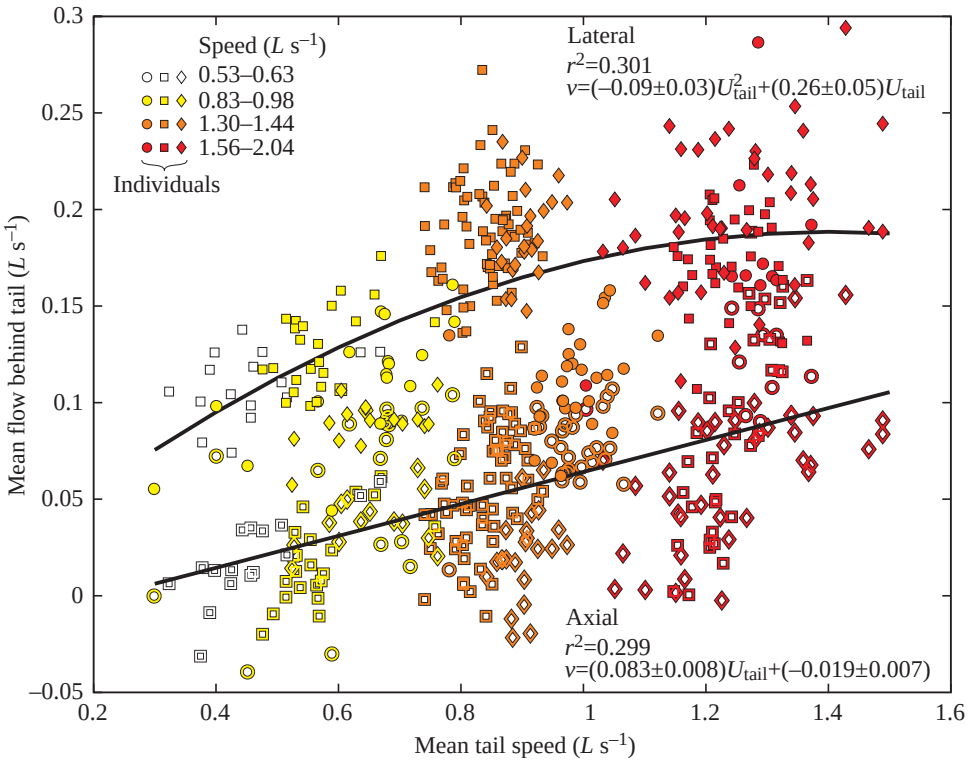

Fig. 7. Mean flow in an 8×8 mm region, 8 mm behind the tail, plotted against the mean tail speed. Filled symbols represent lateral velocities, and open symbols indicate axial velocities. Shades from white to red represent different swimming speeds, and symbol shape indicates different individuals. The linear and quadratic regression lines for axial and lateral velocities, respectively, are shown with thick black lines, and the r^2 values and regression equations are indicated nearby.

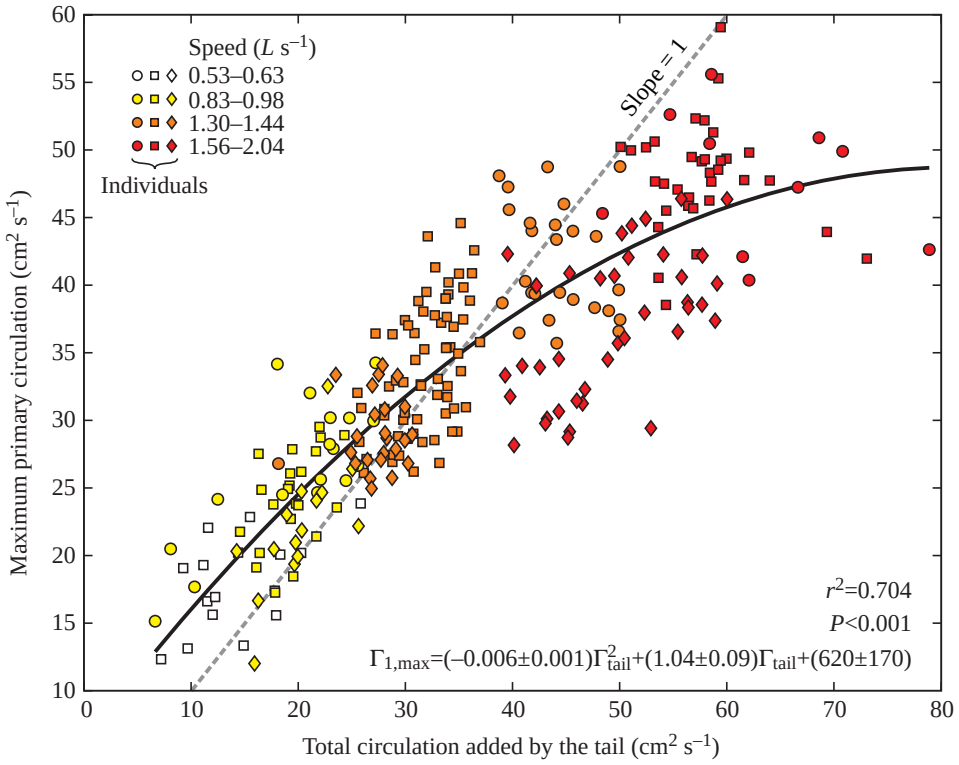

Fig. 8. Maximum circulation value for the primary vortex plotted against the total circulation added by the tail, estimated by equation 10. A quadratic regression line is shown with a thick black line, and a one-to-one relationship is shown with a gray broken line. Shades from white to red represent different swimming speeds, and marker shape indicates different individuals. The P and r^2 values, and the regression equation, are given in the corner.

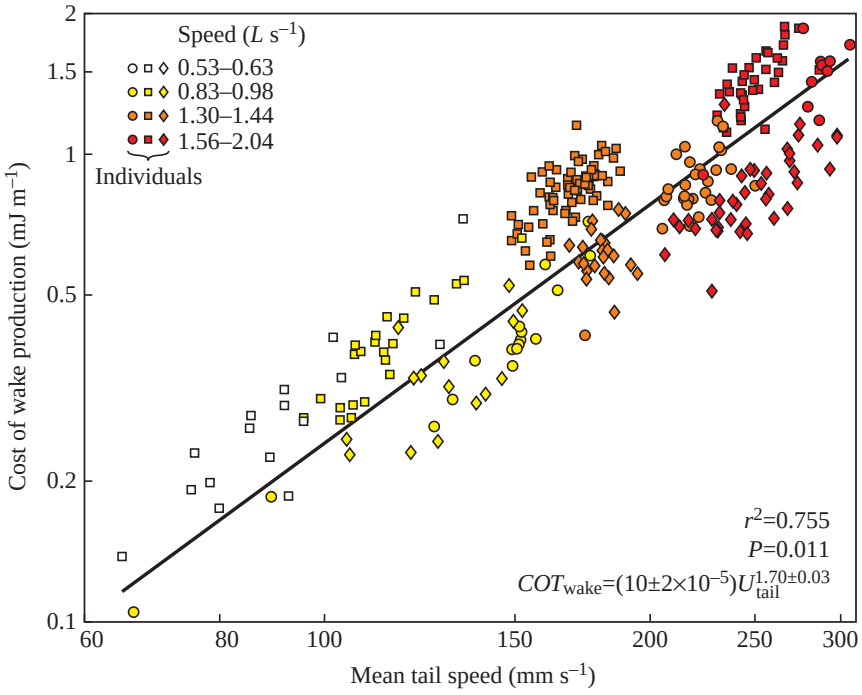

Fig. 9. Log–log plot of the cost of producing the wake against mean tail speed. A linear regression is shown with a thick black line, and the P and r^2 values and the regression equation are given in the corner. Shades from white to red represent different swimming speeds and marker shape indicates different individuals.

(PTOT) is significantly larger than the reactive power (KEBT; P=0.048), while mean lateral PIV power coefficient (PLAT) is not significantly different from the reactive power coefficient (KEBT; P=0.753).

Discussion

This study is the first to combine PIV and detailed body kinematics for a swimming fish. As a result, this study begins to connect the large body of swimming kinematics studies and inviscid flow theories to the growing field of experimental swimming hydrodynamics.

Simultaneous kinematic and PIV data were collected at four different swimming speeds, from ~0.5 to 2 L s^{-1}. The kinematics were consistent with previous data from eels and other anguilliform swimmers (Gillis, 1997, 1998). At all speeds, the wake resembled that described in Part I of this study: laterally directed jets of fluid, separated by regions of vorticity, with little downstream flow (Figs 4, 6). The jet increases in strength at higher swimming speeds and tends to become wider but does not change angle (Fig. 5). Tail tip velocity seems to be the kinematic parameter that most affects the flow in the wake. The circulation of the vortices surrounding the jet increases with increasing tail tip velocity but seems to level off at the higher speeds. Even so, the cost of producing this wake increases exponentially at higher tail velocities, corresponding to higher speeds.

The kinematic data from this study are consistent with Gillis's recent work on eels (Gillis, 1998). For example, at 1.0 L s^{-1}, he observed a tail beat frequency of 2.484±0.007 Hz, a body wave speed of 1.27±0.02 L s^{-1} and a tail tip amplitude of ~0.08 L, compared with the values from this study of 2.61±0.08 Hz, 1.34±0.01 L s^{-1} and 0.059±0.001 L, respectively. Also,

in *Siren intermedia*, a salamander that swims in the anguilliform mode, Gillis (1997) observed a similar use of decreasing angles of attack for increasing swimming speed (Fig. 3A). However, in *Siren*, the proportion of the tail beat with positive angles of attack increases with swimming speed, while for *Anguilla* the proportion decreases (Fig. 3B).

Strouhal number, the ratio of mean tail beat speed to swimming speed, has received increasing attention in recent years as a kinematic parameter that has a strong effect on hydrodynamics (Triantafyllou et al., 1993, 2000; Taylor et al., 2003). Flapping foils reach a peak in efficiency near a Strouhal number of 0.3 (Read et al., 2003), which may be related to the instability of the wake for those flapping parameters (Triantafyllou et al., 1993). Eels, like many other fishes, swim with a tail beat amplitude and frequency near this Strouhal number. In addition, eels maintain a constant Strouhal number within a single swimming speed (Fig. 2) by varying tail beat frequency inversely with amplitude. Amplitude and frequency differences primarily represent individual differences but, because they vary inversely to keep *St* constant, the variation may not affect the hydrodynamics substantially. For example, the individual represented by squares in Fig. 2 consistently chose a higher amplitude and lower frequency than the others. Strouhal number, on the other hand, was the only kinematic parameter that did not show a significant difference between individuals (P=0.860), which probably reflects its hydrodynamic importance.

Because of the physical importance of Strouhal number, it would have been convenient to plot hydrodynamic measurements against it, rather than against swimming speed. Unfortunately, *St* stays constant. Instead, hydrodynamic variables were usually plotted against tail velocity, as in Figs 6–9. Variation in tail velocity at a constant flow speed represents changes in Strouhal number, which should have hydrodynamic consequences. Indeed, in each of these plots, the hydrodynamic variable varies with tail velocity both within and between swimming speeds. If the hydrodynamic variables were plotted against swimming speed alone, the variation within a speed would have been lost.

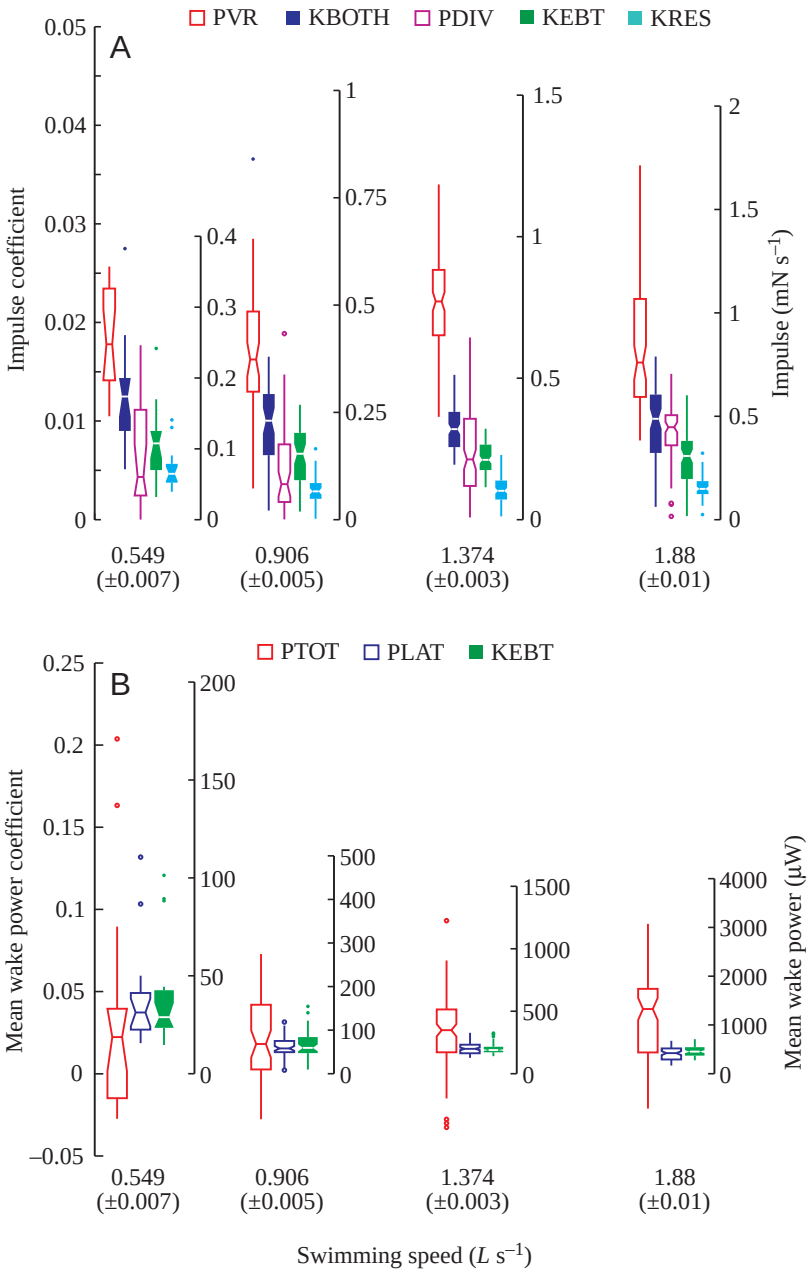

Fig. 10. Comparison of impulse and power estimates at different swimming speeds. Coefficients are shown on the left-hand axes, and dimensional values are shown on the right-hand axes. Boxes are standard statistical box plots, described in detail in Fig. 1. Open boxes represent estimates from PIV, and filled boxes represent estimates from the kinematics. Colors indicate what type of estimate was used. (A) Impulse estimates. (B) Power estimates.

Wake structure

It is intriguing to note that the structure of the eel's wake changes very little over a nearly fourfold change in speed (Fig. 4). While the wake jet increases in strength and tends to increase in size, its angle stays the same, and no substantial changes in the overall formation pattern were observed. Even the jet strength has a tendency to stop increasing above ~1.5 L s^{-1}, as is seen in the comparable jet magnitudes at 1.35 and 1.94 L s^{-1} in Fig. 4 and in two individuals in Fig. 5.

While eels' wakes retain a fairly constant structure over a fourfold speed range, other fishes change their wakes substantially as they change swimming speed. For example, mackerel have been observed to reorient their wake jets by nearly 20° over a twofold speed increase (Nauen and Lauder,

2002a). Additionally, labriform swimmers change the angle and strength of the vortex rings they produce as they swim at higher speeds (Drucker and Lauder, 2000). Bluegill sunfish also change the structure of their wake completely; at low speeds, they generate a single vortex ring per fin beat, on the downstroke, but at high speeds, they generate two on the downstroke and the upstroke (Drucker and Lauder, 2000).

The reason eel wake structure does not change when that of other fishes does may be related to differences in how eels and other fishes balance thrust and drag. As discussed in detail in Tytell and Lauder (2004), all steadily swimming fishes must produce no net forward force; i.e. thrust must equal drag. Other fishes seem to segregate thrust production from drag production, either spatially, by having the thrust-producing fins functionally separated from the rest of the body like propellers, or temporally, by producing pulsatile thrust. This segregation means that evidence of thrust production is visible in the wake, even though, on average, thrust equals the drag on the body. We hypothesized in Part I that eels do not have this segregation and therefore produce no net downstream force within the speed range examined in this study, indicated by the zero axial component of F_{vort} (P=0.989). Thus, the jets must point laterally to maintain zero axial flow, and the reorientation observed in other fishes is not possible. When eels accelerate, the net axial force is no longer zero, and the wake jets do reorient (E.D.T., personal observation).

In this study, however, all eels were swimming steadily, and the morphology of the wake is fairly constant. It might seem that other hydrodynamic variables suggest a change in the wake at the highest speeds observed in this study, or possibly at higher speeds. For example, in Fig. 7, lateral flow behind the tail tends to level off at high swimming speed, and in Fig. 8, Γ_{tail} overestimates primary vortex circulation at speeds higher than 1.8 L s^{-1}. I argue, however, that these effects do not represent a difference in how the wake is generated at high speeds. In the first place, the cost of producing the wake increases at a constant rate as speed increases (Fig. 9). The rate is slower than might be expected from a scaling argument but it does not show any breaks at different speeds. Additionally, the nonlinear relationship in Fig. 8 may not represent a true change in generation mechanism. Fig. 8 was constructed as if the tail was a vortex ring generator. Piston-based vortex ring generators have an effect referred to as 'formation number': a maximum circulation that can be added to a single vortex ring (Gharib et al., 1998). The formation number is the ratio of the distance the piston travels to its diameter. When this value is above 4, no more circulation can be added to a single vortex ring. By analogy, the overestimate of primary vortex circulation at high speeds may represent a similar effect; that the tail cannot add more circulation to the primary vortex above 50 cm^2 s^{-1}. Because an eel is not a piston, it is difficult to estimate a value for a formation number at the tail. Nonetheless, the effect may still exist and may explain the lack of increase in circulation at high swimming speeds. Circulation, in turn, is directly tied to the jet velocity between the vortices. The formation number effect thus may also explain why jet magnitude and lateral flow level off at high speed, without the need to hypothesize a change in generation mechanism.

An empirical description of eel swimming

An empirical description of eel locomotion is useful because it relates simple, easily measured quantities, such as Strouhal number, tail beat frequency or amplitude, to important hydrodynamic variables. Examining discrepancies between empirical relationships and those predicted by theoretical models such as Lighthill's reactive EBT (Lighthill, 1971) and Taylor's resistive model (Taylor, 1952) may also provide physical insight into swimming mechanics.

Dimensionless constants provide the simplest empirical description of eel swimming. Over a Reynolds number range from ~20 000 to 80 000, impulse and power coefficients based on PIV both stay approximately constant. Mean vortex ring impulse coefficient remained at 0.0194±0.0004 across speeds, total power remained at 0.0377±0.0006 and lateral power was somewhat lower (0.0157±0.0003). For a 20 cm eel swimming at 1 L s^{-1}, these coefficients are equivalent to 0.49±0.01 mN s^{-1}, 191±3 μW and 79±2 μW, respectively. The lateral vortex ring force coefficient decreased from 0.14±0.02 at 0.549 L s^{-1} to 0.070±0.003 at 1.88 L s^{-1}, corresponding to forces of 1.1±0.2 mN and 6.3±0.3 mN.

There was a non-significant trend for both power coefficients to decrease at higher speeds, as can be seen in Fig. 10B. Additionally, lateral force coefficients also tended to decrease at higher speeds, because the tail beat frequency increased more slowly than the length-specific swimming speed. In essence, the same impulse was produced over a relatively longer period at high speed, resulting in a lower force coefficient. Data from individuals with a greater size range will be necessary to establish the constancy of impulse coefficients and the trends for power and force coefficients more firmly, but, in a general way, these coefficients can better characterize the hydrodynamic performance of eels during steady swimming than theoretical models. In a recent paper, Schultz and Webb (2002) urge the use of power coefficients, rather than Froude efficiency, as a means of describing swimming performance.

While Froude propulsive efficiency would be useful to estimate, it requires a measurement of thrust, which cannot be estimated due to the lack of axial flow in the wake. However, changes in the cost of producing the wake (Fig. 9), one component of the total cost of transport, may indicate trends in propulsive efficiency. The cost increases as the tail velocity with the exponent 1.48, which is equivalent to cost increasing with swimming speed with the same exponent. If the power coefficient stayed constant, the cost should increase as swimming speed squared, meaning that the cost of producing the wake increases less quickly than might be expected. In fact, power coefficients do tend to decrease slightly (Fig. 10B), possibly indicating an increase in efficiency at higher speeds.

Kinematics can even provide a more detailed picture of the wake structure. For example, at all speeds except the highest, an eel's tail functions like a vortex ring generator (Shariff and

Leonard, 1992), adding circulation to the fluid at a rate proportional to its velocity squared (Fig. 8). Additionally, the jet diameter is consistently about a quarter of the total body wavelength, regardless of the substantial individual variation in body wavelength. Together, these two relationships give a good idea of the wake structure and can also be combined to produce the wake impulse.

Impulse and power estimates

Beyond simply describing the empirical relationship of kinematics and hydrodynamics, a goal of this study was to examine the consistency of different methods of estimating impulse and power, both directly from the wake and from the kinematics alone. From the wake, two methods of estimating impulse were examined. First, the vorticity in the wake was assumed to be part of a small core vortex ring, and the generation impulse for that ring was calculated based on the midline circulation of the ring, according to equations 6, 7. Second, no specific vortical structure was assumed, and the first moment of vorticity, relative to the tail tip, was integrated over the plane, according to equation 8. In comparison, from the kinematics alone, three methods of estimating impulse were explored. Lighthill's reactive EBT (Lighthill, 1971) and blade-element resistive models (e.g. Taylor, 1952; Jordan, 1992) produce force estimates that can be integrated to produce impulse. Additionally, the sum of the two kinematic impulses was compared with the PIV estimates. Power, in turn, was estimated from the PIV data by integrating the kinetic energy flux convected through a plane behind the eel. A 'lateral' power was also constructed in the same way but ignoring the axial components of flow. These estimates were compared with the EBT estimate of power shed into the wake. The resistive model does not account for the way power is shed into the wake and was therefore excluded from the comparison.

Each of these different methods have potential errors from various sources, detailed below. Most of the error from PIV comes from the fact that flow in only a single, horizontal plane was measured. If the geometry of the vortex ring was different from the oval shape that was assumed, the force could be over- or underestimated. However, studies that included multiple orthogonal planes (Drucker and Lauder, 2001; Nauen and Lauder, 2002a) conclude that wake vortex rings are oval shaped, and the force estimated from those vortex rings tended to equal the measured drag force, supporting the validity of this assumption. By contrast, to estimate a total force from the first moment of vorticity, it was assumed that vorticity was the same in all planes over the height of the eel and that there was no vorticity along the other orthogonal axes. Vorticity is actually a vector quantity (Faber, 1995); a horizontal plane allows an estimate of vorticity in the vertical direction. The same studies with orthogonal planes demonstrated that substantial vorticity exists in the other directions (Drucker and Lauder, 2001; Nauen and Lauder, 2002a), probably resulting in an underestimate of total impulse by directly integrating vorticity. Birch and Dickinson (2003), who successfully used the first moment of vorticity to estimate lift and drag on an insect wing, used a system that was configured such that the primary contribution to lift and drag forces was from spanwise vorticity. For the eel, both the measured vertical vorticity and the unmeasured axial vorticity combine to produce lateral forces. The force estimate from the first moment of vorticity does not include this axial vorticity and thus underestimates total force.

PIV power estimates do not require as many assumptions about the structure of the flow as do force and impulse estimates, but there may still be errors because a complete control volume around the eel was not observed. In principle, power should be estimated by taking the difference between the kinetic energy passing through two planes, one upstream of the eel's snout and one downstream of the eel's tail. This method would give an estimate of the rate at which the eel adds energy to the fluid. Because eels will not swim with their heads in the light sheet, it was not possible to obtain the flow upstream of the head. The upstream flow was therefore assumed to be constant and equal to the mean flow velocity. However, due to turbulent effects from the boundary layer, the upstream flow may not be constant and, particularly, may include regions of accelerated or decelerated axial flow due to quasi-streamwise vortices (Robinson, 1991). Very little lateral flow was observed due to the turbulent boundary layer or other effects within the flow tank. If quasi-streamwise vortices do affect the upstream flow, the total PIV power will be affected. In calculating 'lateral' PIV power, all momentum that the eel added to the wake was assumed to be in the lateral direction. This assumption may be justified because the eel's axial momentum was not changing. Therefore, it could not cause the axial fluid momentum to change; it could only cause changes in lateral fluid momentum. Any fluctuations in axial velocity were therefore assumed to be the result of turbulence and were ignored.

These PIV estimates were compared with two types of theoretical models. Both the reactive EBT (Lighthill, 1971) and the resistive model (Taylor, 1952; Blake, 1979) make assumptions about the flow. EBT assumes that viscosity is unimportant, which is typical at high Reynolds number (Faber, 1995), and that the only substantial force comes from the acceleration reaction, not from any quasi-steady resistive drag forces (Lighthill, 1971; Daniel, 1984). The blade-element resistive model includes those forces but not the acceleration reaction. It also makes the assumption that individual segments along the eel's body from its head to its tail do not affect the flow around successive segments. Although this assumption is clearly false, due to the acceleration of fluid down the eel's body (Müller et al., 2001; Tytell and Lauder, 2004), interactions between segments may not cause a substantial change in the forces (Blake, 1979). Calculating wake power using the resistive model explicitly requires violating this assumption, because each fluid element must flow along the body into the wake. Therefore, power was not estimated using the resistive model.

Given those potential sources of error, the different methods

were compared using a three-way mixed model ANOVA. The impulse estimated by assuming that the wake consists of small core vortex rings (PVR), which is hypothesized to be the most accurate following other wake studies (Drucker and Lauder, 1999, 2001; Nauen and Lauder, 2002a), is larger than any other method of estimating impulse (P<0.001 in all cases). Neither the reactive model, the resistive model nor their sum predicts as much impulse as observed in the wake. Thus, these simple models do not fully describe the complexity of eel swimming. Nonetheless, both reactive and resistive impulses are important, making up 33±1% and 16.5±0.5%, respectively, of the estimated PIV impulse. The remaining ~50% may come from more complex fluid interactions along the body, including three-dimensional effects and vortex shedding along the dorsal and anal fin.

By contrast, inviscid theory predicts the 'lateral' power with a striking degree of accuracy. Both the time course and the magnitude of this power are successfully estimated by EBT alone (Fig. 10; Table 2). This power was calculated using only the lateral flow component, due to the impossibility of obtaining a complete control volume around the eel and the presence of turbulent flow structures that are primarily directed in the axial direction. EBT estimates wake power as the rate at which fluid kinetic energy at the tail tip is convected into the wake (Lighthill, 1971). This estimate is separate from the estimate of force and thus it is possible for one to be accurate when the other is not, as observed. Therefore, the power output can be described accurately by a simple theoretical model, but, despite this correspondence, neither a reactive model nor a quasi-steady resistive model fully capture the complexity of force output for a swimming eel.

I would like to thank George Lauder, who provided many useful comments and suggestions as this project has evolved, and Christoffer Johanssen, Peter Madden, Matt McHenry and Emily Standen, who were helpful for advice throughout the project. Michelle Chevalier helped collect and digitize some of the kinematic data. I also owe thanks to Laura Farrell, who maintained the animals used in this study. This research was supported by the NSF under grants IBN9807021 and IBN0316675 to George Lauder.

References

Aleyev, Y. G. (1977). *Nekton*. The Hague: Junk.

Anderson, J. M. (1996). Vortex control for efficient propulsion. *Ph.D. Thesis.* Dept of Ocean Eng., Massachusetts Institute of Technology.

Birch, J. M. and Dickinson, M. H. (2003). The influence of wing–wake interactions on the production of aerodynamic forces in flapping flight. *J. Exp. Biol.* **206**, 2257-2272.

Blake, R. W. (1979). The mechanics of labriform locomotion. I. Labriform locomotion in the angelfish (*Pterophyllum eimekei*): an analysis of the power stroke. *J. Exp. Biol.* **82**, 255-271.

Breder, C. M. (1926). The locomotion of fishes. *Zoologica* **4**, 159-297.

Daniel, T. L. (1984). Unsteady aspects of aquatic locomotion. *Am. Zool.* **24**, 121-134.

Donley, J. M. and Dickson, K. A. (2000). Swimming kinematics of juvenile kawakawa tuna (*Euthynnus affinis*) and chub mackerel (*Scomber japonicus*). *J. Exp. Biol.* **203**, 3103-3116.

Drucker, E. G. and Lauder, G. V. (1999). Locomotor forces on a swimming fish: three-dimensional vortex wake dynamics quantified using digital particle image velocimetry. *J. Exp. Biol.* **202**, 2393-2412.

Drucker, E. G. and Lauder, G. V. (2000). A hydrodynamic analysis of fish swimming speed: wake structure and locomotor force in slow and fast labriform swimmers. *J. Exp. Biol.* **203**, 2379-2393.

Drucker, E. G. and Lauder, G. V. (2001). Locomotor function of the dorsal fin in teleost fishes: experimental analysis of wake forces in sunfish. *J. Exp. Biol.* **204**, 2943-2958.

Faber, T. E. (1995). *Fluid Dynamics for Physicists.* Cambridge: Cambridge University Press.

Fincham, A. M. and Spedding, G. R. (1997). Low cost, high resolution DPIV for measurement of turbulent fluid flow. *Exp. Fluids* **23**, 449-462.

Gharib, M., Rambod, E. and Shariff, K. (1998). A universal time scale for vortex ring formation. *J. Fluid Mech.* **360**, 121-140.

Gillis, G. B. (1997). Anguilliform locomotion in an elongate salamander (*Siren intermedia*): effects of speed on axial undulatory movements. *J. Exp. Biol.* **200**, 767-784.

Gillis, G. B. (1998). Environmental effects on undulatory locomotion in the American eel *Anguilla rostrata*: kinematics in water and on land. *J. Exp. Biol.* **201**, 949-961.

Gray, J. (1933). Studies in animal locomotion. I. The movement of fish with special reference to the eel. *J. Exp. Biol.* **10**, 88-104.

Hart, D. P. (2000). PIV error correction. *Exp. Fluids* **29**, 13-22.

Hoerner, S. F. (1965). *Fluid-Dynamic Drag*. Brick Town, NJ: Hoerner Fluid Dynamics.

Jayne, B. C. and Lauder, G. V. (1995). Speed effects on midline kinematics during steady undulatory swimming of largemouth bass, *Micropterus salmoides*. *J. Exp. Biol.* **198**, 585-602.

Jordan, C. E. (1992). A model of rapid-start swimming at intermediat Reynolds number: Undulatory locomotion in the chaetognath *Sagitta elegans*. *J. Exp. Biol.* **163**, 119-137.

Lighthill, M. J. (1960). Note on the swimming of slender fish. *J. Fluid Mech.* **9**, 305-317.

Lighthill, M. J. (1971). Large-amplitude elongated-body theory of fish locomotion. *Proc. R. Soc. Lond. A* **179**, 125-138.

Marey, E. J. (1895). *Le Mouvement.* Paris: Masson.

McCutchen, C. W. (1977). Froude propulsive efficiency of a small fish, measured by wake visualisation. In *Scale Effects in Animal Locomotion* (ed. T. J. Pedley), pp. 339-363. London: Academic Press.

Milliken, G. A. and Johnson, D. E. (1992). *Analysis of Messy Data. 1. Designed Experiments.* London: Chapman and Hall.

Milliken, G. A. and Johnson, D. E. (2001). *Analysis of Messy Data. 3. Analysis of Covariance*. Boca Raton, FL: CRC Press.

Müller, U. K., van den Heuvel, B.-L. E., Stamhuis, E. J. and Videler, J. J. (1997). Fish foot prints: morphology and energetics of the wake behind a continuously swimming mullet (*Chelon labrosus risso*). *J. Exp. Biol.* **200**, 2893-2906.

Müller, U. K., Smit, J., Stamhuis, E. J. and Videler, J. J. (2001). How the body contributes to the wake in undulatory fish swimming: flow fields of a swimming eel (*Anguilla anguilla*). *J. Exp. Biol.* **204**, 2751-2762.

Nauen, J. C. and Lauder, G. V. (2002a). Hydrodynamics of caudal fin locomotion by chub mackerel, *Scomber japonicus* (Scombridae). *J. Exp. Biol.* **205**, 1709-1724.

Nauen, J. C. and Lauder, G. V. (2002b). Quantification of the wake of rainbow trout (*Oncorhynchus mykiss*) using three-dimensional stereoscopic digital particle image velocimetry. *J. Exp. Biol.* **205**, 3271-3279.

Pedley, T. J. and Hill, S. J. (1999). Large-amplitude undulatory fish swimming: fluid mechanics coupled to internal mechanics. *J. Exp. Biol.* **202**, 3431-3438.

Quinn, G. P. and Keough, M. J. (2002). *Experimental Design and Data Analysis for Biologists*. Cambridge: Cambridge University Press.

Read, D. A., Hover, F. S. and Triantafyllou, M. S. (2003). Forces on oscillating foils for propulsion and maneuvering. *J. Fluids Struct.* **17**, 163-183.

Robinson, S. K. (1991). Coherent motions in the turbulent boundary layer. *Annu. Rev. Fluid Mech.* **23**, 601-639.

Rosen, M. W. (1959). *Waterflow About A Swimming Fish*. China Lake, CA: US Naval Ordnance Test Station.

Schultz, W. W. and Webb, P. W. (2002). Power requirements of swimming: do new methods resolve old questions? *Integ. Comp. Biol.* **42**, 1018-1025.

Shariff, K. and Leonard, A. (1992). Vortex Rings. *Annu. Rev. Fluid Mech.* **24**, 235-279.

Taylor, G. (1952). Analysis of the swimming of long and narrow animals. *Proc. R. Soc. Lond. A* **214**, 158-183.

Taylor, G., Nudds, R. and Thomas, A. L. R. (2003). Flying and swimming animals cruise at a Strouhal number tuned for high power efficiency. *Nature* **425**, 707.

Triantafyllou, G. S., Triantafyllou, M. S. and Grosenbaugh, M. A. (1993). Optimal thrust development in oscillating foils with application to fish propulsion. *J. Fluids Struct.* **7**, 205-224.

Triantafyllou, M. S., Triantafyllou, G. S. and Yue, D. K. P. (2000). Hydrodynamics of fishlike swimming. *Annu. Rev. Fluid Mech.* **32**, 33-53.

Tytell, E. D. and Lauder, G. V. (2004). The hydrodynamics of eel swimming. I. Wake structure. *J. Exp. Biol.* **207**, 1825-1841.

Videler, J. J. and Hess, F. (1984). Fast continuous swimming of two pelagic predators, saithe (*Pollachius virens*) and mackerel (*Scomber scombrus*): a kinematic analysis. *J. Exp. Biol.* **109**, 209-228.

Webb, P. W. (1973). Kinematics of pectoral fin propulsion in *Cymatogaster aggregata*. *J. Exp. Biol.* **59**, 697-710.

Webb, P. W. (1975). Hydrodynamics and energetics of fish propulsion. *Bull. Fish. Res. Bd. Can.* **190**, 1-159.

Webb, P. W. (1988). Steady swimming kinematics of tiger musky, an esociform accelerator, and rainbow trout, a generalist cruiser. *J. Exp. Biol.* **138**, 51-69.

Webb, P. W. (1991). Composition and mechanics of routine swimming of rainbow trout, *Oncorhynchus mykiss*. *Can. J. Fish. Aquat. Sci.* **48**, 583-590.

Webb, P. W. (1992). Is the high cost of body caudal fin undulatory swimming due to increased friction drag or inertial recoil. *J. Exp. Biol.* **162**, 157-166.

Webb, P. W. and Fairchild, A. G. (2001). Performance and maneuverability of three species of teleostean fishes. *Can. J. Zool.* **79**, 1866-1877.

Weihs, D. (1972). A hydrodynamical analysis of fish turning maneuvers. *Proc. R. Soc. Lond. B* **182**, 59-72.

Wu, T. Y. (1971). Hydromechanics of swimming propulsion. Part 1. Swimming of a two-dimensional flexible plate at variable forward speeds in an inviscid fluid. *J. Fluid Mech.* **46**, 337-355.